Effect of flood hydrograph duration, magnitude, and shape on bed-load transport dynamics

Authors C. B. Phillips[1], K. M. Hill[2,4], C. Paola[3,4], M. B. Singer[5], and D. J. Jerolmack[6]

[1]Civil and Environmental Engineering, Northwestern University, Evanston, IL.
[2]Civil, Environmental, and Geo-Engineering, University of Minnesota, Minneapolis, MN.
[3]Earth Sciences, University of Minnesota, Minneapolis, MN.
[4]St. Anthony Falls Laboratory, University of Minnesota, Minneapolis, MN.
[5]Earth and Ocean Sciences, Cardiff University, Cardiff, UK.
[6]Earth and Environmental Sciences, University of Pennsylvania, Philadelphia, PA.

Corresponding author: Colin B. Phillips (colinbphillips@gmail.com)

Key Points

(1) Laboratory experiments reveal that cumulative bed load flux for a flood is linearly related to the flow impulse (integrated potential transport capacity).

(2) For an equivalent flow impulse, transient and steady floods transport the same total bed-load sediment flux.

(3) Flood duration, magnitude and shape affect bed load flux in terms of their contribution to the flow impulse but are otherwise interchangeable for well sorted gravel.

Abstract

Bed load sediment transport is an inherently challenging process to measure within a river, which is further complicated by the typically transient nature of the hydrograph. Here we use laboratory experiments to explore how sediment flux under transient – unsteady and intermittent – flow differ from those under steady flow. For a narrow unimodal sediment distribution, we calculated fluid stress and measured sediment flux for a range of hydrograph durations, magnitudes, shapes, and sequences. Within a hydrograph, we find considerable variability in sediment flux for a given stress above the threshold for motion. However, cumulative bed-load flux resulting from a flood scales linearly with the integrated excess transport capacity (flow impulse). This scaling indicates that, to first order, flow magnitude, duration, shape, and sequence are only relevant to bedload flux in terms of their contribution to the total flow impulse, in agreement with prior field results. The flood impulse represents a quantitative parameter through which the effects of transient flow on coarse sediment transport may be parsed.

Plain language summary

Mountain river floods produced from snowmelt can last months but remain relatively shallow, while floods resulting from storms are often shorter in duration and deeper. These floods have, in a sense, different “shapes” and “sizes” determined by their environment and climate. We performed laboratory experiments to understand how these flood shapes and sizes affect the amount of sediment they can move, a key precursor to understanding how rivers and flooding impact the landscapes in which they reside. Our experiments show that if one accounts for the forcing of the flood in a physically based manner, there is no difference between floods of different shapes and sizes in terms of how much sediment they move. We suggest that these results may make floods easier to characterize when modeling landscapes.

1. Introduction

Under steady flow, the rate of bed-load transport in rivers is a stochastic process that varies both spatially and temporally due to turbulent fluid-stress fluctuations, bed topography, and granular structure. Field and laboratory observations demonstrate that variability within the grain size distribution (Wilcock and McArdell, 1997), the magnitude of upstream sediment supply (Singer,

2010; Recking, 2012), mobility (Wilcock, 1998), and structural arrangement (Church et al., 1998; Strom et al., 2004; Zimmermann et al., 2010; Marquis and Roy, 2012; Houssais et al., 2015) of river-bed sediments affect the flux resulting from an applied flow stress (Recking, 2013). Stream hydrology is assumed to be a primary control on the magnitude and duration of the applied bed stress. In natural environments, river flows are rarely steady as gravel-bed rivers typically experience flows that exceed the threshold required for sediment motion only during floods. Strictly speaking, natural floods violate the assumptions of steady and uniform flow required for current sediment transport calculations. The transience of natural hydrographs presents a barrier to applying the mechanistic understanding of sediment transport dynamics developed under steady flows in laboratory experiments to natural rivers.

At timescales of a single flood event (from the initiation of motion to the cessation of bed material transport) to timescales of multiple flood events, it remains an open question how steady and transient flows differ in terms of their effects on channel morphology and bed load sediment dynamics. Observations within the natural environment have led to the attribution of various phenomena to aspects of transient flow such as: the degree of vertical and spatial bed grain size segregation (armor) (Reid and Laronne, 1995), the amount of grain protrusion (Yager et al., 2012), channel bed complexity (Singer and Michaelides, 2014; Whiting and Stamm, 1995), and variability in the threshold of motion (Turowski, 2011). However, for flows in natural rivers it is exceedingly difficult to distinguish between phenomena that occur under steady flow and those that require a transient hydrograph. The majority of transient-flow laboratory experiments explore the role of magnitude and duration (Hassan et al., 2006; Bombar et al., 2011; Humphries et al., 2012; Mao, 2012), flow sequence (Humphries et al., 2012; Guney et al., 2013; Waters and Curran 2015), and to a lesser degree the time between floods (intermittency) (Ferrer-Boix and Hassan, 2015; Masteller and Finnegan, 2017) on the development of bed-surface texture in mixed unimodal or bimodal sediment beds. When compared with their accompanying steady flow counterparts, these experiments collectively paint a complex picture of the intermixing of gravel-bed morphology, adjustment timescales, and mixed grain-size mobility thresholds (e.g. Wilcock, 1998; Wilcock and Crowe, 2003; Parker et al. 2008) with changing flow rates at various durations. Using a well sorted gravel sediment with constant sediment feed and a sequence of identical hydrographs, Wong and Parker (2006) determined that downstream of a

short inlet boundary layer, the sediment flux adjusted to track the variations in the hydrograph. The use of sediment beds with broad, mixed, or bimodal grain-size distributions complicates these findings considerably (An et al., 2017). With more complex grain-size distributions the magnitude of the peak and duration of the rising and falling limbs have the potential to create bed states with a higher threshold of motion (Mao, 2012). These complex bed states induce a variety of hysteresis loops between flow and sediment flux (Mao, 2012; Humphries et al., 2012; Guney et al., 2013), making it difficult to predict the instantaneous flux using equations developed under steady flow conditions (Guney et al., 2013; Lee et al., 2004). However, despite the shortcomings of most transport equations to compute instantaneous transport, they can be modified to provide reasonable predictions of the total flux (Lee et al., 2004; Wong and Parker, 2006; Humphries et al., 2012), suggesting that this complexity may not be intractable over complete flood hydrographs.

Linking sediment transport dynamics to landscape evolution requires developing physically based metrics capable of bridging the gaps between discrete floods, sequences of hydrographs that define a regional climate, and the long-term approximation of hydrographs within landscape evolution models (Paola et al., 1992; Lague, 2014; Phillips and Jerolmack, 2016). Recent field results on the transport of marked tracer cobbles demonstrate that despite substantial hydrologic variability, average particle displacement scales linearly with the integrated excess shear velocity, or impulse (Phillips et al., 2013; Phillips and Jerolmack, 2014; Imhoff and Wilcox, 2016), suggesting that to first order the effects of flow transience may be accounted for through the quantification of the flow impulse. However, substantial variability exists within these data as the cumulative impulse is scaled down to that of a single flood. Here we report results from laboratory flume experiments at St. Anthony Falls Laboratory (SAFL) at the University of Minnesota under transient flow to quantitatively compare the flow impulse to bed load flux for individual floods and sequences of floods (Phillips, 2018). These experiments explore a parameter space of magnitude and duration for four geometrically simplified flood shapes. We demonstrate that even with a well sorted unimodal sediment bed, there is considerable variability in instantaneous flux-stress relationships for different flood shapes. At the same time, we show that, when integrated over a flood hydrograph, flows of equivalent total impulse transport the

same total sediment flux. Finally, we show how the impulse concept can be used to normalize floods to facilitate the comparison of both steady and unsteady floods.

2. Experiments

2.1 Experimental design

Our experiments do not attempt to recreate a natural flood regime in the lab (Paola et al., 2009). Rather they are designed to understand how transport in transient flows might differ from steady flows and how the components of transient flows, unsteadiness and intermittence, potentially contribute to different sediment dynamics. We explore these components of flow transience through the use of sequences of geometrically simplified steady and unsteady floods where the effects of flood peak magnitude, duration, and shape on sediment transport dynamics can be independently investigated (Figure 1a-b). For clarity, in this Letter, we use the term 'flood' to refer to a distinct transport event, from the period where particles start moving to when they stop. We use 'flood shape' to describe the time dependence of the flow magnitude for a single flood, and the phrase 'flood sequence' to refer to multiple sequential discrete floods. Flood sequences of steady or unsteady floods represent the intermittent component of transient flows (Figure 1c). To compare the effects of these components on particle transport, we normalize each flood by its potential fluid-derived transport capacity, or impulse (T_*):

$$T_* = \int_{t_s}^{t_f} (U_\tau^2 - U_{\tau c}^2)^{3/2}\, dt / gD^2 \qquad (1)$$

where U_τ is the shear velocity (m/s), $U_{\tau c}$ is the threshold shear velocity for sediment motion (m/s), g is the acceleration due to gravity (m/s^2), D is a representative grain size (m) taken here as the geometric mean, and t_f and t_s are the starting and ending times of the flood, respectively. We note that equation (1) is valid only for flows able to transport sediment ($U_\tau > U_{\tau c}$). We then compare runs of equivalent T_* and varying magnitude, duration, and shape in terms of their measured dimensionless cumulative sediment flux (Q*):

$$Q_* = \int_{t_s}^{t_f} (q_b) dt / D^2 \qquad (2)$$

where q_b is the volumetric sediment flux per unit width (m^2/s). Normalizing each flood by T_* accounts for the expected average behavior under steady flow, effectively representing all flows as square waves, because T_* does not distinguish between flow magnitude, duration, or shape.

We performed two experiments to isolate the effects of transient flow at the flood scale. The first experiment is comprised of sequences of floods with constant peak hydrograph magnitudes, while sequences of floods in the second experiment had variable peak magnitudes (Figure 1c). In the first type of experiments, we ran sequences (12-20) of intermixed steady and unsteady floods with equal T_* and equivalent hydrograph peak magnitude. To explore a parameter space of peak magnitude and duration (Figure 1b) we ran additional sequences with increased or decreased flood magnitude and/or flood duration (see supporting information and Figure S2). The second set of experiments was designed to test the effects of sequences of floods (6-12) with variable magnitude and duration (Figure 1c lower panel). These experiments allow us to contrast sets of floods with high magnitude and short duration against those of low magnitude and longer duration, but with equivalent T_*. Throughout both experiments, the bed within the test section of the flume was not disturbed or altered; it was allowed to evolve.

2.2 Experimental setup

We conducted the experiments at SAFL in a 30 m by 0.5 m sediment and water feed flume (Figure S1). Water discharge (Q, m^3/s) was controlled using a variable speed pump that discharged into a head tank before flowing over a weir and entering the 22.5 m long experimental section of the flume. The flume data acquisition system was set up to record measurements every second of water surface elevation and the mass of sediment accumulating at the end of the flume. A narrow unimodal mixture of sediment (with geometric mean diameter D=7.2 mm and standard deviation 1.2 mm) was fed 2.5 m downstream of the inlet weir via sediment feeder during all periods when bed shear stress exceeded the critical threshold for motion. We note that we used the same sediment and flume, though with a different setup, as used in Wong and Parker (2006), Wong et al. (2007), and Hill et al. (2010). For each run, water discharge was brought from baseflow up to the peak flow rate and then back to baseflow. In the case of unsteady runs, the rate of rise and fall depends on the shape of the hydrograph (Figure 2a & S2). This results in a temporally variable and often rapidly changing flow depth within the flume. We kept the slope of the sediment bed at steady state, no net aggradation or erosion, by feeding sediment for each flood such that $Q_{*in} \approx Q_{*out}$, resulting in a proportional feed system. To achieve this, we adjusted the sediment feed rate for each flood (Figure S3) such that sediment

was supplied only during periods where the flood was capable of transporting sediment (see supporting information for additional details).

Cumulative time series of sediment mass leaving the flume were continuously recorded as the sediment deposited in a submerged suspended basket attached to a load cell (Interface SMT2-500 N load cell, Figure S1). Water surface elevation (1 Hz, 1 mm accuracy) was measured at three locations within the flume using ultrasonic transducers (Massa mPulse M-5000, Figure S1). To reduce experimental noise within the time series all data were smoothed using a Savitzky-Golay filter (7 second window, 2nd order polynomial). Laser sheet scans of bed topography (1 mm vertical and horizontal accuracy) were taken between sets of floods after the flow was turned off and the flume had been allowed to drain the surface layer. The sediment mass, bed topography scans, and water surface elevation data were used to derive the remaining variables. Sediment flux (q_s, kg/s) represents the derivative of the cumulative mass time series over an eight-second moving window. Water surface slope (S) was estimated from the first and third sensors by linear regression (see supporting information for further explanation). Flow depth (h, m) was estimated by differencing the intermittent bed topography scans from the water surface elevation time series. The sediment bed slope remained relatively constant (S_{mean}=9.3×10^{-3} and S_{SD}=7.4×10^{-4}) throughout both series of experiments, and differences in bed elevation (ΔZ, mm) between scans for the location where h was calculated were small (ΔZ_{mean}=-0.1 mm and ΔZ_{SD}=1.5 mm). Flow velocity (U, m/s) was calculated as $U=Q/(hb)$ where b is the flume width. Shear stress (τ, Pa) was approximated using the procedure outlined in Vanoni and Brooks (1975) to account for sidewall effects using time series of: h, S, Q, and U. We calculated shear velocity as $U_\tau = \sqrt{\tau/\rho}$ and Shields stress as $\tau_* = \tau/(\rho_s - \rho)gD$, where ρ_s is sediment density (2650 kg/m^3), and ρ is the water density. Additional methodological notes are available in the supporting information.

3. Results

For each flood, measured time series of water surface elevation and sediment mass were used to derive time series of flow discharge, velocity, depth, water surface slope, and sediment flux (Figure 2). Time series data are available for 209 runs totaling 23.5 hours of experiments and 2,155 kg of transported sediment with: peak U_τ=0.087-0.12 (τ_*=0.065-0.12), ratios of peak

206 $U_\tau/U_{\tau c}$=1.08-1.5 (τ_*/τ_{*c}=1.18-2.23), total durations ranging from 2.5-30 min, durations above the
207 threshold of motion of 0.6-29.1 min (Figure 1c), and cumulative flux masses per flood ranging
208 from 1-32 kg. We examine the results from these experiments first within individual floods and
209 second at the scale of a complete flood and multiple flood sequences.
210
211 **3.1 Within a flood**
212 Within each flood there is considerable variability between sediment flux and stress; however we
213 find that to first order the stress flux data can be described by a bed-load transport equation of the
214 form $q_*=K(\tau_*-\tau_{*c})^\alpha$ (Meyer-Peter and Müller, 1948; Wong and Parker, 2006) (Figure 2b), where
215 q_* is the dimensionless volumetric sediment flux. Here we fix the exponent at α=1.5 (Wong and
216 Parker, 2006; Wong et al., 2007). Allowing α to vary produces only minor improvements that do
217 not provide a strong justification for the additional free parameter. We note that similar
218 formulations of the flux law (see Table 1 in Lajeunesse et al., 2010) provide equally convincing
219 fits to the data. For any given run, we observe a small range of coefficients, average threshold
220 stresses, and in some cases thresholds of initiation and cessation of transport (Figure 2b & c) that
221 change between rising and falling hydrograph limbs. We observe counter-clockwise hysteresis in
222 sediment flux primarily when the flow changes rapidly. The hysteresis occurs over short
223 timescales and represents a small fraction of the sediment flux. Hysteresis in sediment flux and
224 hysteresis in the threshold of motion were not always coincident in the same flood.
225
226 **3.2 Flood and sequence scale**
227 Examining the flux data at the sequence scale we find that all steady and transient floods follow
228 a similar trend (Figure 3a). There is considerable scatter in the flux data; however, the mean of
229 the data cloud is well described by a single transport law of the same power law form fit to data
230 from individual floods (Figure S4a), except those at the highest stresses, where data are sparse.
231 We fit the transport law to all data where $q_* \geq 0$ and $\tau_* \geq 0.045$ by least-squares regression,
232 yielding parameters for the coefficient (K=5.0) and threshold of motion (τ_{*c}=0.055). These
233 cutoffs for τ_* and q_* arise from the sensitivity of the load cell and noise associated with the
234 experimental set up of the sediment weighing basket. We also separated the bulk flux data into
235 steady and unsteady floods as well as by flood shape to assess if these subsets of the data
236 behaved differently. Inspection of the distributions of residuals determined from the transport

law (fit in Figure 3a) for each subset yield minimal discernable differences between them (Figure S4a-c).

To compare flows of different shape, peak magnitude, and duration we computed T_* for each flood (eq. 1). Since the flux data can be represented with a single transport law (Figure 3a), we compute equations 1 and 2 for all runs using a single value for the threshold of motion ($U_{\tau c}$=0.08 m/s). Additionally, we use a single value for grain size (D=0.0072 m) in both equations 1 and 2. After computing both integrated parameters we find that to first order the T_* parameter collapses the flux data onto a single linear trend (Figure 3b). All floods but one are within a factor of 1.5 of the mean trend. Within this data collapse, there is no systematic variation in the data with respect to flood magnitude, duration, or shape.

4. Discussion and Conclusions

The degree of complexity present in the flux data for each run (Figure 2 a-c) is evident in the hysteresis present in both the calculated threshold of motion and magnitude of flux on the rising and falling limbs of unsteady flows. Hysteresis loops in these experiments occur for floods with rapidly changing hydraulic stresses and are typically absent in runs when the flow gradually increases or decreases. The short timescales over which the hysteresis is present for both rising and falling flows indicate a lag between the calculated instantaneous stress via the depth-slope product and the response of the bed, suggesting there may be a minimum time required to average the flow conditions in order to compute a representative stress via the depth-slope product. Hysteresis is common in transient flow experiments (Hassan et al., 2006; Mao, 2012), however the short run times and well-sorted gravel bed presented here preclude most of the commonly reported mechanisms. The narrow grain size distribution reduces grain scale sorting, armoring, and size selective transport, which even under steady flows can result in differentially mobile populations of bed sediments (Wilcock and McArdell, 1997). Additionally, the short duration of competent flow limits the effects of phenomena with longer timescales of adjustment such as bedforms and sediment texture (Ferrer-Boix and Hassan, 2014). In terms of total flux, though, the observed hysteresis represents a small fraction of the sediment transported in a flood.

Interestingly, and perhaps surprisingly, this intra-flood variability is not evident at the scale of a single flood, in which T_* collapses the Q_* data onto a single linear relation (Figure 3b). In terms of their cumulative sediment flux, the linear scaling between T_* and Q_* indicates that unsteady runs are equivalent to steady runs. The scatter in cumulative flux about the mean trend does not vary systematically with flood duration, peak magnitude, shape, or sequence, indicating its source is not associated with flood type or flow transience. Additionally, the data collapse indicates that for the parameter space explored here, flow magnitude and duration are relevant only in how they contribute to T_*. Under these conditions the sediment flux does not depend on the flow history, indicating that the sequence of runs did not exert substantial control on the total flux. This flow history independence indicates a memoryless system under the given conditions. In terms of flood intermittency, the linear scaling indicates that not only can a series of smaller events' impulses be summed to equal a run with a larger impulse, but that the sequence of the smaller impulses of various shapes does not matter (Figure 1 & 3).

The linear scaling between T_* and Q_* and its implications are contingent on the validity of the non-linear flux law relating U_τ or τ_* to q_* that forms the basis of the impulse (Equation 1). However, these experiments demonstrate that this relation need be valid only at an integral scale to recover a reasonable collapse of the data (Figure 3b), though this integral scale remains to be determined in natural systems. To place these results into a broader context, we summarize two important limitations of these experiments: (1) limited flow durations and (2) limited range of shear velocity. The limited flow durations simulated here preclude the observation of morphologic structures with longer time scales of formation or adjustment, if they are not already precluded by the narrow grain size distribution. The range in peak stress magnitudes is comparable to previous similar experiments (Hassan et al., 2006; Mao, 2012; Humphries et al., 2012) and represents approximately half the reach average transport capacity ($U_\tau/U_{\tau c}$) observed within natural bed load rivers (Phillips and Jerolmack, 2016). In practice, this limited range of peak stresses may be less restricting as bed-load flux laws are more robust for $U_\tau >> U_{\tau c}$ (Capart and Fraccarollo, 2011; Recking et al., 2012). Meaningful deviations from the flux law are more likely for floods with low stress magnitudes near the threshold of motion, where sufficiently longer averaging timescales are required (Recking et al., 2012; Houssais et al., 2015). In such cases, dynamic interactions between the bed and the flow may be capable of altering $U_{\tau c}$. This

includes processes such as bed dilation due to high stresses or compaction from constant forcing above and below the threshold of motion (Charru et al. 2004; Marquis and Roy, 2012; Houssais et al., 2015; Masteller and Finnegan, 2017). However, such dynamic interactions were not observed within the data.

The largest unknown is the role of the grain size distribution, as the narrow one used here greatly reduced the textural, morphological, and granular adjustments that could have occurred (see Ferrer-Boix and Hassan, 2014) within the flume (by design). Introducing a wider grain-size distribution with particle size dependent mobility (common for broad or bimodal grain size distributions) would likely require the impulse in equation (1) to be modified to reflect a fractional transport equation (Wilcock and Crowe, 2003). The narrow grain size distribution was chosen to isolate the influence of the hydrograph; however, one of the implications of our experiments is that the grain-size distribution potentially represents the largest source of variability (Hassan et al., 2006). It remains an open question which grain-size distribution (bimodal, broad, or mixed transport), when paired with transient flow, has the greatest potential to add memory to the system.

Despite the limitations, our results may be more general than they initially seem. These experiments support the surprising conclusion that the total sediment mass transported is insensitive to the details of the transient hydraulic forcing, as has also been observed for bed load tracers in natural rivers (Phillips et al., 2013; Imhoff and Wilcox, 2016). Additionally, these results are (in spirit) the same treatment of the hydrograph embodied in the simplest physically based models of landscape evolution (see Paola et al., 1992), where the full complexity of a hydrograph is replaced by the bankfull flood (average, see Phillips and Jerolmack, 2016) multiplied by an intermittency factor. This similarity is by no means a complete test of such treatments, due to our simplified size distribution, other missing processes, and scale differences, yet it does reinforce the notion present in both landscape evolution models and field tracer studies that substantial complexity need not preclude a simple treatment.

Acknowledgements

Research was supported by a NSF-Postdoctoral Fellowship (EAR-1349776), the National Center for Earth Surface Dynamics 2 (NCED2, EAR-1246761), and the NSF INSPIRE program (EAR-1344280). We thank S. Harrington and K. Francois-King for outstanding laboratory assistance. These experiments were performed at St. Anthony Falls Laboratory and benefitted from the technical support of: C. Ellis, R. Gabrielson, E. Steen, B. Erickson, and R. Christopher. We thank L. Hsu and J. Myers for assistance with data publication. Finally, we thank S. Chartrand and an anonymous reviewer for comments that increased the clarity of this manuscript. Experimental data and processing codes are publicly available through the SEAD repository (http://doi.org/10.5967/M0S180MK).

References

An, C., Fu, X., Wang, G., & Parker, G. (2017). Effect of grain sorting on gravel bed river evolution subject to cycled hydrographs: Bed load sheets and breakdown of the hydrograph boundary layer. *Journal of Geophysical Research: Earth Surface*, *122*(8), 2016JF003994. https://doi.org/10.1002/2016JF003994

Bombar, G., Elci, S., Tayfur, G., Guney, S., & Bor, A. (2011). Experimental and Numerical Investigation of Bed-Load Transport under Unsteady Flows. *Journal of Hydraulic Engineering-Asce*, *137*(10), 1276–1282. https://doi.org/10.1061/(ASCE)HY.1943-7900.0000412

Capart, H., & Fraccarollo, L. (2011). Transport layer structure in intense bed-load. *Geophysical Research Letters*, *38*(20), L20402. https://doi.org/10.1029/2011GL049408

Charru, F., Mouilleron, H., & Eiff, O. (2004). Erosion and deposition of particles on a bed sheared by a viscous flow. *Journal of Fluid Mechanics*, *519*, 55–80. https://doi.org/10.1017/S0022112004001028

Church, M., Hassan, M. A., & Wolcott, J. F. (1998). Stabilizing self-organized structures in gravel-bed stream channels: Field and experimental observations. *Water Resources Research*, *34*(11), 3169–3179. https://doi.org/10.1029/98WR00484

Ferrer-Boix, C., & Hassan, M. A. (2014.). Influence of the sediment supply texture on morphological adjustments in gravel-bed rivers. *Water Resources Research*, *50*(11), 8868–8890. https://doi.org/10.1002/2013WR015117

Ferrer-Boix, C., & Hassan, M. A. (2015), Channel adjustments to a succession of water pulses in gravel bed rivers, *Water Resources Research*, 51, 8773–8790, doi:10.1002/2015WR017664.

Guney, M. S., Bombar, G., & Aksoy, A. O. (2013). Experimental Study of the Coarse Surface Development Effect on the Bimodal Bed-Load Transport under Unsteady Flow Conditions. *Journal of Hydraulic Engineering*, *139*(1), 12–21. https://doi.org/10.1061/(ASCE)HY.1943-7900.0000640

Hassan, M. A. & Church, M. (2000). Experiments on surface structure and partial sediment transport on a gravel bed. Water Resources Research, 36, 1885-1895, doi.org/10.1029/2000WR900055

368 Hassan, M. A., Egozi, R., & Parker, G. (2006). Experiments on the effect of hydrograph
369 characteristics on vertical grain sorting in gravel bed rivers. *Water Resources Research, 42*, 15. https://doi.org/200610.1029/2005WR004707
371 Hill, K. M., DellAngelo, L., & Meerschaert, M. M. (2010). Heavy-tailed travel distance in gravel
372 bed transport: An exploratory enquiry. *Journal of Geophysical Research*, *115*, F00A14.
373 https://doi.org/10.1029/2009JF001276
374 Houssais, M., Ortiz, C. P., Durian, D. J., & Jerolmack, D. J. (2015). Onset of sediment transport
375 is a continuous transition driven by fluid shear and granular creep. *Nature*
376 *Communications*, *6*, 6527. https://doi.org/10.1038/ncomms7527
377 Humphries, R., Venditti, J. G., Sklar, L. S., & Wooster, J. K. (2012). Experimental evidence for
378 the effect of hydrographs on sediment pulse dynamics in gravel-bedded rivers. *Water*
379 *Resources Research*, *48*, 15. https://doi.org/201210.1029/2011WR010419
380 Imhoff, K. S., & Wilcox, A. C. (2016). Coarse bedload routing and dispersion through tributary
381 confluences. *Earth Surface Dynamics*, *4*(3), 591–605.
382 https://doi.org/https://doi.org/10.5194/esurf-4-591-2016
383 Lague, D. (2014). The stream power river incision model: evidence, theory and beyond. *Earth*
384 *Surface Processes and Landforms*, *39*(1), 38–61. https://doi.org/10.1002/esp.3462
385 Lajeunesse, E., Malverti, L., & Charru, F. (2010). Bed load transport in turbulent flow at the
386 grain scale: Experiments and modeling. *Journal of Geophysical Research*, *115*, 16.
387 https://doi.org/201010.1029/2009JF001628
388 Lee, K. T., Liu, Y.-L., & Cheng, K.-H. (2004). Experimental investigation of bedload transport
389 processes under unsteady flow conditions. *Hydrological Processes*, *18*(13), 2439–2454.
390 https://doi.org/10.1002/hyp.1473
391 Mao, L. (2012). The effect of hydrographs on bed load transport and bed sediment spatial
392 arrangement. *Journal of Geophysical Research-Earth Surface*, *117*.
393 https://doi.org/10.1029/2012JF002428
394 Marquis, G. A., & Roy, A. G. (2012). Using multiple bed load measurements: Toward the
395 identification of bed dilation and contraction in gravel-bed rivers. *Journal of Geophysical*
396 *Research*, *117*(F1), F01014. https://doi.org/10.1029/2011JF002120
397 Masteller, C. C., & Finnegan, N. J. (2017). Interplay between grain protrusion and sediment
398 entrainment in an experimental flume. *Journal of Geophysical Research: Earth Surface*,
399 *122*(1), 2016JF003943. https://doi.org/10.1002/2016JF003943
400 Meyer-Petter, E., & Muller, R. (1948). Formulas for bed-load transport. In *Proceedings* (pp. 39–
401 64). Stockholm, Sweden.
402 Paola, C., Heller, P. L., & Angevine, C. L. (1992). The large-scale dynamics of grain-size
403 variation in alluvial basins, 1: Theory. *Basin Research*, *4*, 73–90.
404 Paola, C., Straub, K., Mohrig, D., & Reinhardt, L. (2009). The unreasonable effectiveness of
405 stratigraphic and geomorphic experiments. *Earth-Science Reviews*, *97*(1–4), 1–43.
406 https://doi.org/10.1016/j.earscirev.2009.05.003
407 Parker, G., & Wilcock, P. R. (1993). Sediment Feed and Recirculating Flumes: Fundamental
408 Difference. *Journal of Hydraulic Engineering*, *119*(11), 1192–1204.
409 https://doi.org/10.1061/(ASCE)0733-9429(1993)119:11(1192)
410 Parker, G., & Wilcock, P. R. (1995). Closure to "Sediment Feed and Recirculating Flumes:
411 Fundamental Difference" by Gary Parker and Peter R. Wilcock. *Journal of Hydraulic*
412 *Engineering*, *121*(3), 293–294. https://doi.org/10.1061/(ASCE)0733-
413 9429(1995)121:3(293)

Parker, G., Hassan, M., & Wilcock, P. R. (2008). Adjustment of the bed surface size distribution of gravel-bed rivers in response to cycled hydrographs. *Gravel-Bed Rivers VI: From Process Understanding to River Restoration*, 241–285.

Phillips, C. B. (2018) Transient Flows Unimodal Sediment, SEAD Repository, doi.org/10.5967/M0S180MK

Phillips, C. B., & Jerolmack, D. J. (2014). Dynamics and mechanics of bed-load tracer particles. *Earth Surface Dynamics*, *2*(2), 513–530. https://doi.org/10.5194/esurf-2-513-2014

Phillips, C. B., & Jerolmack, D. J. (2016). Self-organization of river channels as a critical filter on climate signals. *Science*, *352*(6286), 694–697. https://doi.org/10.1126/science.aad3348

Phillips, C. B., Martin, R. L., & Jerolmack, D. J. (2013). Impulse framework for unsteady flows reveals superdiffusive bed load transport. *Geophysical Research Letters*, *40*(7), 1328–1333. https://doi.org/10.1002/grl.50323

Recking, A. (2012). Influence of sediment supply on mountain streams bedload transport. *Geomorphology*, *175–176*, 139–150. https://doi.org/10.1016/j.geomorph.2012.07.005

Recking, A. (2013). An analysis of nonlinearity effects on bed load transport prediction. *Journal of Geophysical Research: Earth Surface*, *118*(3), 1264–1281. https://doi.org/10.1002/jgrf.20090

Reid, I., & Laronne, J. B. (1995). Bed Load Sediment Transport in an Ephemeral Stream and a Comparison with Seasonal and Perennial Counterparts. *Water Resources Research*, *31*(3), 773–781. https://doi.org/10.1029/94WR02233

Singer, M. B. 2010. Transient response in longitudinal grain size to reduced gravel supply in a large river. Geophysical Research Letters 37: L18403, doi:18410.11029/12010gl044381, 10.1029/2010gl044381.

Singer, M. B., & Michaelides, K. (2014). How is topographic simplicity maintained in ephemeral dryland channels? *Geology*, *42*(12), 1091–1094. https://doi.org/10.1130/G36267.1

Strom, K., Papanicolaou, A. N., Evangelopoulos, N., & Odeh, M. (2004). Microforms in gravel bed rivers: Formation, disintegration, and effects on bedload transport. *Journal of Hydraulic Engineering-Asce*, *130*(6), 554–567. https://doi.org/10.1061/(ASCE)0733-9429(2004)130:6(544)

Turowski, J. M., Badoux, A., & Rickenmann, D. (2011). Start and end of bedload transport in gravel-bed streams. *Geophysical Research Letters*, *38*, 5. https://doi.org/201110.1029/2010GL046558

Vanoni, V. A., and N. H. Brooks (1975), *Sedimentation Engineering*. Manuals and Reports on Engineering Practice No. 54, ASCE, 745, Am. Soc. Civ. Eng., Reston, Va.

Waters, K. A., & Curran, J. C. (2015). Linking bed morphology changes of two sediment mixtures to sediment transport predictions in unsteady flows. *Water Resources Research*, *51*(4), 2724–2741. https://doi.org/10.1002/2014WR016083

Whiting, P. J., & Stamm, J. (1995). The hydrology and form of spring-dominated channels. *Geomorphology*, *12*(3), 233–240. https://doi.org/10.1016/0169-555X(95)00006-Q

Wilcock, P. R. (1998). Two-Fraction Model of Initial Sediment Motion in Gravel-Bed Rivers. *Science*, *280*(5362), 410–412. https://doi.org/10.1126/science.280.5362.410

Wilcock, P. R., & Crowe, J. C. (2003). Surface-based Transport Model for Mixed-Size Sediment. *Journal of Hydraulic Engineering*, *129*(2), 120.

Wilcock, P. R., & McArdell, B. W. (1997). Partial transport of a sand/gravel sediment. *Water Resources Research*, *33*(1), 235–245. https://doi.org/10.1029/96WR02672

Wong, M., Parker, G., DeVries, P., Brown, T. M., & Burges, S. J. (2007). Experiments on dispersion of tracer stones under lower-regime plane-bed equilibrium bed load transport. *Water Resources Research*, *43*, 23. https://doi.org/200710.1029/2006WR005172

Wong, M., & Parker, G. (2006a). One-dimensional modeling of bed evolution in a gravel bed river subject to a cycled flood hydrograph. *Journal of Geophysical Research*, *111*, 20. https://doi.org/200610.1029/2006JF000478

Wong, M., & Parker, G. (2006b). Reanalysis and correction of bed-load relation of Meyer-Peter and Muller using their own database. *Journal of Hydraulic Engineering-Asce*, *132*(11), 1159–1168. https://doi.org/10.1061/(ASCE)0733-9429(2006)132:11(1159)

Yager, E. M., Turowski, J. M., Rickenmann, D., & McArdell, B. W. (2012). Sediment supply, grain protrusion, and bedload transport in mountain streams. *Geophysical Research Letters*, *39*. https://doi.org/10.1029/2012GL051654

Zimmermann, A., Church, M., & Hassan, M. A. (2010). Step-pool stability: Testing the jammed state hypothesis. *Journal of Geophysical Research: Earth Surface*, *115*(F2). https://doi.org/10.1029/2009JF001365

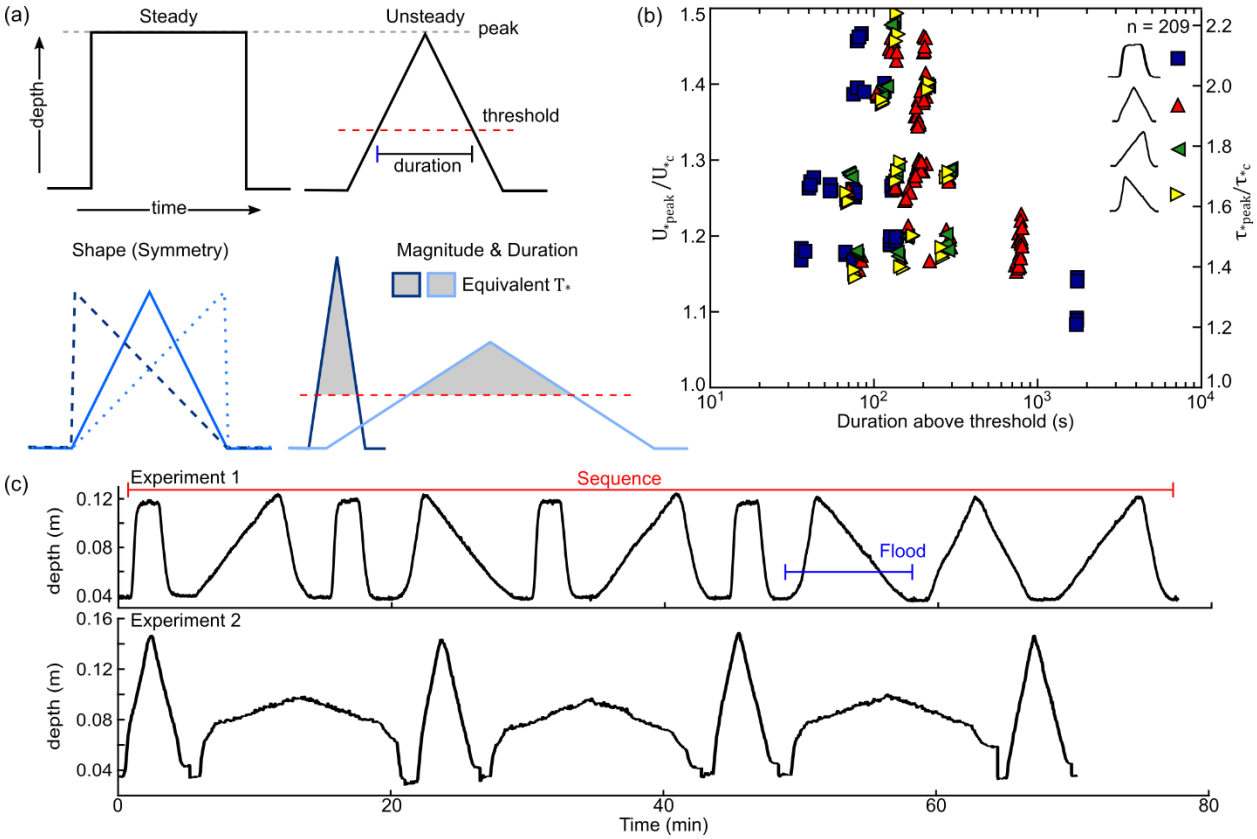

Figure 1. Experimental design. (a) Schematic hydrographs of steady (upper left) and unsteady (upper right) symmetric flows, and three unsteady flow shapes (lower left) explored in these experiments. (lower right) Schematic hydrographs showing two flows of equal impulse with different peak magnitude and duration. (b) Experimental parameter space of flow durations above the threshold of motion and dimensionless peak magnitude in shear velocity and shields stress normalized by the threshold of motion. Legend denotes experimental flood shape next to symbol. (c) Examples of experimental sequences. (top panel) Hydrograph sequence of steady and unsteady flows with equal peak magnitude and impulse for each run. (lower panel) Hydrograph of unsteady runs with alternating peak magnitude and duration.

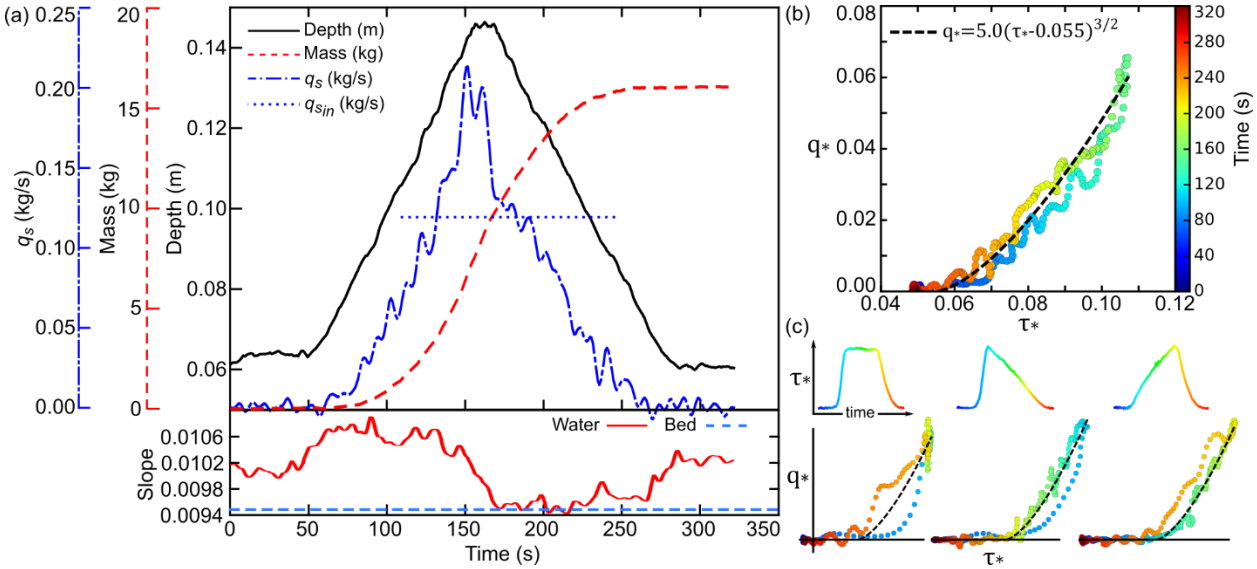

Figure 2. Experimental data. (a) Primary data are flow depth (black line), cumulative sediment mass (red dashed line), sediment feed rate (blue dotted line), and sediment flux (blue dash dot line). The subplot shows the water surface slope throughout the flood (red line) and the post flood bed surface slope (dashed line). (b) Dimensionless bed load flux and Shields stress for the run shown in (a), where color represents the experimental run time. The dashed black line represents a fitted bed load transport law. (c) Examples of flux stress relations for the other three flood shapes. The top row shows the flow hydrograph in time and stress with the color of the line corresponding to the approximate time location of the flux data in the bottom row. The bottom row shows sediment flux and Shields stress and the dashed black line represents the flux law in (b). For these schematic examples flux and stress are on the same scale for all three, while time is compressed by a factor ~1.3 for the asymmetric flood shapes.

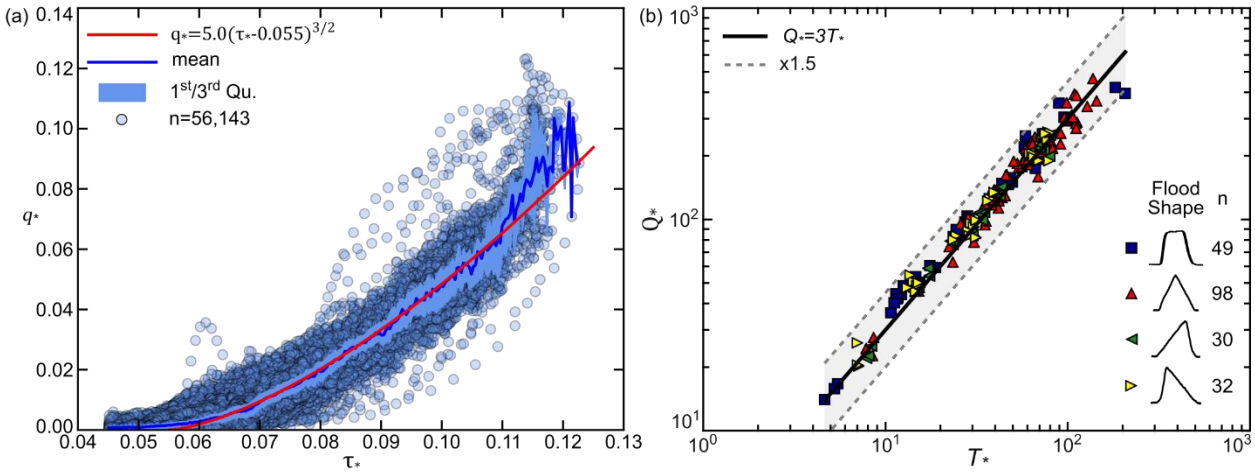

Figure 3. (a) Dimensionless sediment transport rate and Shields stress for all experimental runs for $q_* \geq 0$ and $\tau_* \geq 0.045$. The blue line represents the average, shaded regions are the first and third quartiles, and the red line is the fitted sediment transport flux law. (b) Dimensionless impulse (T_*) versus dimensionless cumulative sediment flux (Q_*) for all runs. Example hydrographs for each run are depicted next to the symbols alongside the number of runs for that flood shape. The black line is a linear trend line fit through the origin, and the grey dashed lines represent a factor of 1.5 times the linear trend.